J Comput Neurosci (2007) 22:313–326
DOI 10.1007/s10827-006-0015-5

Simulation of high-frequency sinusoidal electrical block of mammalian myelinated axons

Niloy Bhadra · Emily A. Lahowetz · Stephen T. Foldes · Kevin L. Kilgore

Received: 27 February 2006 / Revised: 9 November 2006 / Accepted: 11 December 2006 / Published online: 3 January 2007

Abstract High frequency alternating current (HFAC) sinusoidal waveforms can block conduction in mammalian peripheral nerves. A mammalian axon model was used to simulate the response of nerves to HFAC conduction block. Sinusoidal waveforms from 1 to 40 kHz were delivered to eight simulated axon diameters ranging from 7.3 to 16 μm. Conduction block was obtained between 3 to 40 kHz. The minimum peak to peak current at which block was obtained, defined as the block threshold, increased with increasing frequency. Block threshold varied inversely with axon diameter. Upon initiation, the HFAC waveform produced one or more action potentials. These simulation results closely parallel previous experimental results of high frequency motor block of the rat sciatic and cat pudendal nerve. During HFAC block, the axons showed a dynamic steady state depolarization of multiple nodes, strongly suggesting a depolarization mechanism for HFAC conduction block.

Keywords Nerve conduction block · High frequency alternating current · Nerve simulation · Sinusoidal currents · Depolarization

Action Editor: Karen Sigvardt

N. Bhadra · E. A. Lahowetz · S. T. Foldes · K. L. Kilgore
Department of Biomedical Engineering, Case Western Reserve University, Cleveland, Ohio, USA

N. Bhadra (✉) · K. L. Kilgore
Department of Orthopaedics, MetroHealth Medical Center, 2500 MetroHealth Drive, Hamann 601, Cleveland, OH 44109, Ohio
e-mail: nxb26@cwru.edu

K. L. Kilgore
Department of Veterans Affairs, Rehabilitation Research and Development Service, Cleveland, Ohio

Introduction

Undesirable hyper-activity of neurons characterizes many diseases and results in pathological motor or sensory effects. Blocking these action potentials (APs) could help alleviate pain or stop unwanted motor effects such as muscle spasms and spasticity. High-frequency alternating current (HFAC), applied directly to the nerve, has been shown to produce a quick-acting, quick reversing conduction block with a minimum of side effects (Tanner, 1962; Woo and Campbell, 1964; Bowman and McNeal, 1986; Kilgore and Bhadra, 2004; Tai et al., 2005a; Bhadra and Kilgore, 2005; Williamson and Andrews, 2005; Bhadra et al., 2006). A review of this literature was presented elsewhere (Kilgore and Bhadra, 2004).

Several key features of high frequency motor block had been identified through randomized and repeated in-vivo experiments on the rat sciatic nerve (Bhadra and Kilgore, 2005). Voltage-controlled HFAC sinusoidal waveforms from 10 to 30 kHz induced a complete and reversible motor block at all frequencies. The block threshold, defined as the voltage below which complete block was not obtained, increased linearly with increasing waveform frequency in the rat. Similar results have been obtained in the cat pudendal nerve, where motor block was achieved over the range of 1 to 30 kHz (Bhadra et al., 2006).

In the rat sciatic nerve, three sequential phases were identified in the block onset (Bhadra and Kilgore, 2005): an onset response consisting of a muscle twitch with a peak 1 to 8 times that of a normal twitch, a variable period of repetitive firing and a final steady state of complete or partial block (Bhadra and Kilgore, 2005). The onset activity (the first two phases) had a characteristic relationship in the amplitude-frequency space: repetitive firing was minimized at the highest frequencies and highest amplitudes (Bhadra and Kilgore, 2005). In some trials, complete block occurred following

Table 1

Author/Year	Species	Waveform	Block frequency (kHz)	Proof of conduction block
Woo and Campbell (1964)	Frog/Cat	? Sine	20	Nerve recording
Bowman and McNeal (1986)	Cat	Square	4 to 10	Nerve recording
Kilgore and Bhadra (2004)	Frog	Sine	1 to 20	Distal stimulation
Williamson and Andrews (2005)	Rat	Sine	10 to 20	Distal stimulation
Bhadra and Kilgore (2005)	Rat	Sine	10 to 30	Distal stimulation
Bhadra et al. (2006)	Cat	Sine	1 to 30	Distal stimulation

a single normal-sized muscle twitch. However, block was never obtained without any onset activity. Single fiber recordings in cats showed that nerves fired briefly at 700–800 Hz in response to pulse trains of 4 to 10 kHz (Bowman and McNeal, 1986). Their results indicated that there was a bimodal response to the amplitude of the HFAC, with progressively higher amplitudes initially increasing, and then decreasing, the firing rate and duration of firing. These experimental findings regarding the onset activity have not been accurately predicted by previous mammalian modeling of HFAC block (Williamson and Andrews, 2005). The onset response is a key issue that needs to be addressed if HFAC conduction block is to be implemented in clinical applications.

The mechanism by which HFAC blocks nerve conduction has not been determined conclusively. When stimulation is applied in the 0.1 to 1 kHz range, it is possible to produce a fatigue type of block, caused by muscle fatigue or by depletion of the neuromuscular junction transmitter (Solomonow et al., 1983; Sawan et al., 1996). However, at higher frequencies, a true localized nerve conduction block is produced. This was convincingly demonstrated by single-fiber recordings (Bowman and McNeal, 1986) and through the use of distal stimulation to the nerve between the blocking electrode and the neuromuscular junction (Woo and Campbell, 1964; Bowman and McNeal, 1986; Kilgore and Bhadra, 2004; Williamson and Andrews, 2005; Bhadra and Kilgore, 2005; Bhadra et al., 2006). Table 1 shows a summary of findings from various authors who used a method to differentiate nerve conduction block from a fatigue type of block.

The aim of the present study was to understand the fundamental characteristics of the nerve response to HFAC waveforms at frequencies greater than 1 kHz. Investigators are just beginning to utilize mathematical models of the nerve membrane in order to develop an understanding of this phenomenon. Rattay (1990) showed an example of HFAC nerve conduction block at 2 kHz in an unmyelinated Hodgkin-Huxley model (Hodgkin and Huxley, 1952). Tai et al. has presented sine wave block in an unmyelinated Hodgkin-Huxley model (at a temperature of 18.5°C) (Tai et al., 2005c). Williamson and Andrews (2005) performed simulations in three mammalian axon models, using sinusoidal waveforms. Only one model, the Schwarz-Reid-Bostock (SRB) model, demonstrated conduction block from 5 to 20 kHz. One of the other two models showed block only above 50 kHz and the other model exhibited discontinuities between 6 and 7 kHz. In addition, an amphibian model showed block only under restricted circumstances. Given the recent experimental data in frogs (Kilgore and Bhadra, 2004), rats (Bhadra and Kilgore, 2005) and cats (Tai et al., 2005a; Bhadra et al., 2006), it is clear that block occurs experimentally over the range of 5 to 30 kHz. Therefore, of these four models, only the SRB model demonstrated any accuracy in predicting the characteristics of HFAC block.

Modeling of high-frequency conduction block using a mammalian axon model was previously reported (Kilgore and Bhadra, 2004), using the McIntyre, Richardson and Grill (MRG) model (McIntyre et al., 2002), and block was demonstrated with a 5 kHz sinusoid. The present simulation study was conducted to expand the investigation of HFAC block using the MRG model to determine if it was capable of predicting recently published experimental results (Williamson and Andrews, 2005; Bhadra and Kilgore, 2005; Bhadra et al., 2006). The MRG model is a topologically detailed mammalian axonal model based on experimental human, cat and rat data. Topological parameters were derived from cat and rat data, while channel parameters were obtained from human data (McIntyre et al., 2002). Richardson (2000) previously compared three topological axon models and concluded that the double-cable MRG model gave reliable responses for higher frequencies (in the range of 100 Hz). No model has been specifically built for modeling HFAC block. It is appreciated that the choice of model may influence some of the results obtained (Williamson and Andrews, 2005). This manuscript presents the simulation results from the MRG model when subjected to sinusoidal HFAC over a wide range of frequencies, amplitudes, axon diameters and electrode distances. Our analysis of the simulation results is particularly focused on examining the onset phenomenon and elucidating the mechanism of HFAC block.

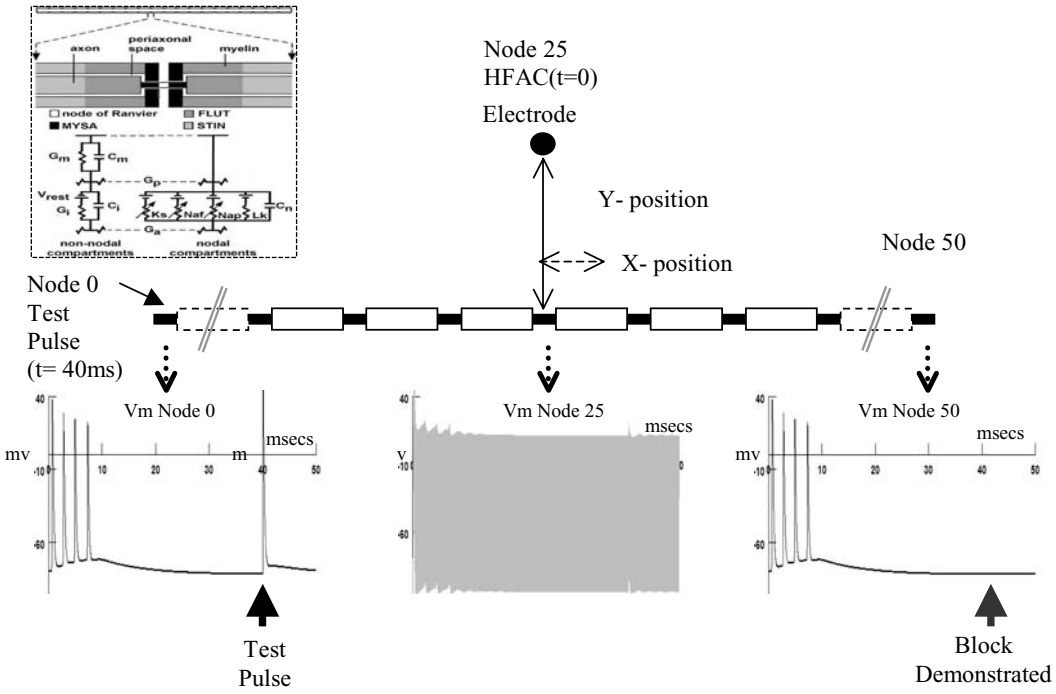

Fig. 1 The myelinated axon model used to simulate sinusoidal high frequency block. A 51 node model is shown with an extracellular electrode placed opposite the central node (X position) at a distance of 1 mm from the axon (Y position). The bottom three panels show transmembrane voltages for nodes 0, 25, and 50 for a 50 ms simulation run. The simulation starts at $t = 0$ with a 10 kHz HFAC sinusoid at 1.154 mA amplitude (2 μA above block threshold) in a 10 μm fiber. The HFAC initiates 4 APs at the onset before reaching a dynamic steady state (transmembrane voltage in node 25 fluctuates in phase with the HFAC sinusoid but maintains an average depolarized value). A test pulse is then injected at node 0 at $t = 40$ ms. This test pulse causes an action potential at node 0 (left panel), which is blocked, as demonstrated by the absence of an AP at node 50 (right panel). The inset shows a schematic of the MRG model (used with permission, McIntyre et al., 2002)

Methods

MRG model

Computer simulations were carried out in Neuron (version 5.8), a nerve simulation software (Hines and Carnevale, 1997). The double-cable mammalian axon model (MRG model) (McIntyre et al., 2002) consisted of quantitatively defined equivalent electrical circuits for both the node and internode regions of the axon (Richardson et al., 2000; McIntyre et al., 2002) (inset in Fig. 1). The nodal circuit consisted of a parallel combination of a nonlinear fast sodium conductance, a nonlinear persistent sodium conductance, a nonlinear slow potassium conductance, a linear leakage conductance, and a membrane capacitance. The internode region was modeled as a circuit composed of two layers of linear components. The specific parameters used were from (McIntyre et al., 2002) and are summarized in Table 2. All equations used in the model have been described by (McIntyre et al., 2002). The model incorporated axon diameters between 7.3 to 16 μm and these diameters had specific topological lengths for all segments, based on experimental data. As a result, a global scaling factor between axon diameter and segment lengths was not used in the MRG model. The model was solved using backward Euler implicit integration with a time step of 0.001–0.005 ms.

Simulation protocols

A 51 node model of the axon was used in all cases (except as noted below). An external electrode was modeled as a single point source over the central node (node 25) (Fig. 1) and placed in an infinite homogenous isotropic medium (resistivity $= 500$ Ω-cm) (Richardson et al., 2000). A current-controlled zero-mean sinusoidal waveform was generated at this electrode (with the first half-cycle being anodic). Current values are reported in this paper as peak-to-peak currents. The amplitude of the blocking waveform was varied in a binary search pattern (with a resolution of 1 μA) to find the minimum current at which block occurred, termed the block threshold. An internal electrode at one end of the axon (node 0) was used to generate a test pulse after the blocking current had been delivered for 40 ms. Preliminary modeling demonstrated that the block was stable within 30 ms. Successful block was defined as the condition where no action potential propagated to the node at the opposite end of the axon (node 50).

Table 2

Node length	1 μm
Myelin attachment paranode length	3 μm
Main paranode length	46 μm
Internodal section length (×6)	175.2 μm
Nodal capacitance	2 μF/cm^2
Internodal capacitance	2 μF/cm^2
Myelin capacitance	0.1 μF/cm^2
Axoplasmic resistivity	70 Ω-cm
Periaxonal resistivity	70 Ω-cm
Myelin conductance	0.001 S/cm^2
Myelin attachment paranode conductance	0.001 S/cm^2
Main segment paranode conductance	0.0001 S/cm^2
Internode segment conductance	0.0001 S/cm^2
Maximum fast Na^+ conductance	3 S/cm^2
Maximum slow K^+ conductance	0.08 S/cm^2
Maximum persistent Na^+ conductance	0.01 S/cm^2
Nodal leakage conductance	0.007 S/cm^2
Na^+ Nernst potential	50 mV
K^+ Nernst potential	− 90 mV
Leakage reversal potential	− 90 mV
Rest potential	− 80 mV
Temperature	37°C

The main variables that were individually modulated were; sinusoidal frequency, axon diameter, electrode-to-axon distance, and the position of the block electrode longitudinally over the axon (Fig. 1). Modeling was performed for: (1) determination of block thresholds, (2) characterization of the onset response, (3) characterization of the mechanism of block and (4) determination of single action potential thresholds (activation thresholds). Different values and ranges of test variables were used for these groups and are summarized in Table 3. Block threshold was used as a standard measure across all variables under test.

Characterization of the onset phenomenon was accomplished by recording the number of onset APs during the first 500 ms of HFAC initiation. The onset phenomenon was analyzed for amplitudes between zero and four times the block threshold. An amplitude step size of 0.02 × block threshold was used from zero to block threshold and a step size of 0.2 × block threshold was used from block threshold to 4 times block threshold. Ten times block threshold was also tested.

The block mechanism was investigated through the collection of multiple sets of data over time and space. A 51 node, 10 μm axon was used and three sets of measurements were collected for all 51 nodes over a time interval equivalent to two cycles of the sinusoidal waveform at an amplitude equal to block threshold for each frequency (block thresholds varied with frequency). This was performed at the end of 40 ms when the block was dynamically stable. The measurements collected were: (i) transmembrane voltage, (ii) fast sodium, persistent sodium, slow potassium, capacitance and leakage currents and (iii) gating parameters h (fast sodium), m (fast sodium), mp (persistent sodium), and s (slow potassium). These results were analyzed using a space plot of each variable (with the node number on the x-axis). In order to examine the dynamic steady state existing along the axon, the value of each variable at each node was determined by averaging over two sinusoidal cycles. This analysis was carried out post-simulation and therefore had no effect on the simulation runs or on the block outcomes.

Results

Block thresholds and HFAC frequency

Conduction block was consistently obtained for all frequencies tested above 3 KHz and for all axon diameters. Examples are shown in Figs. 1 and 2. The thresholds increased

Table 3

	Number of nodes	Axon diameters	Sinusoidal frequency range	Electrode to axon distances	Other variables changed
1(a) Block thresholds	51	7.3, 8.7, 10, 11.5, 12.8, 14, 15, and 16 μm	2 to 40 kHz (2 kHz spacing) + 3 kHz	1 mm	
1(b) Block thresholds	51	10 μm	4, 10, 20, 30, and 40 kHz	0.1, 0.5, 1, 1.5, and 2 mm	
1(c) Block thresholds	51	10 μm	10 kHz	0.1, 0.5, 1, 1.5, and 2 mm	X-position 11 positions
2. Onset phenomenon	51	7.3 and 16 μm	4, 10, 20, 30, and 40 kHz	1 mm	Amplitude 0 to 4 times Block threshold
3(a) Block mechanism	51	10 μm	4, 10, 20, 30, and 40 kHz	0.1, 0.5, 1, 1.5, and 2 mm	
3(b) Block mechanism	51 and 201	7.3, 10 and 16 μm	10 kHz	1 mm	Block threshold multiples
4. Single action potentials	51	10 μm	4 to 40 kHz (2 kHz spacing) + 3 kHz	1 mm	

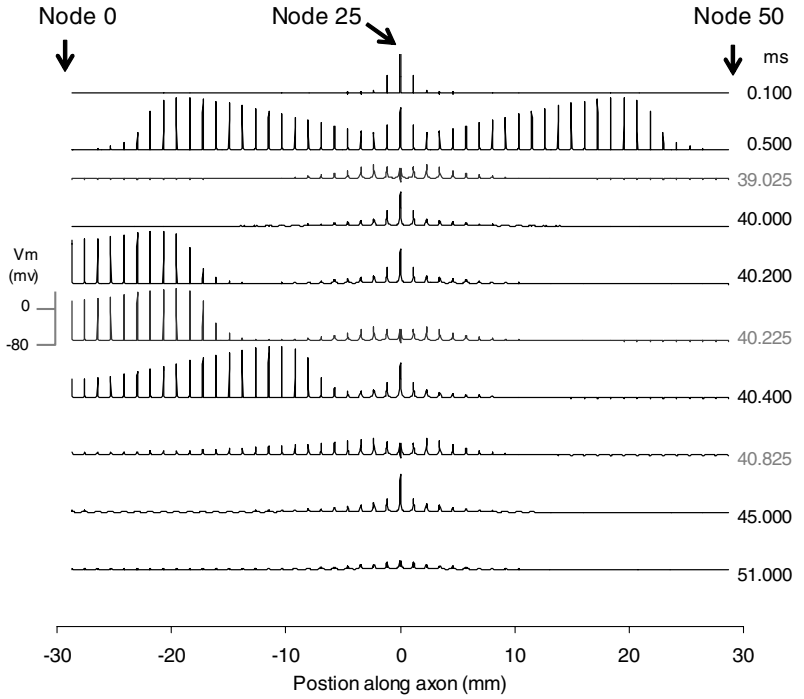

Fig. 2 A stackedh space plot of a 20 kHz HFAC sinusoid block at 1.244 mA (block threshold) in a 10 μm axon with 1 mm electrode-to-axon distance. The transmembrane voltages of all axonal sections (nodes and internodes) are plotted versus axon length in mm. The simulation time is shown on the right of each plot. At 0 ms the block turns on and initiates four action potentials. Only the first AP is shown propagating to both ends of the axon (0.5 ms). There is incremental depolarization over 19 nodes as the HFAC continues, which reaches a dynamic steady state in those nodes by 40 ms (peak depolarization occurs at node 25). A test pulse is delivered at 40 ms from the left and is blocked in the central zone. By 45 ms there is no AP conducted to the right. Extra plots are shown for 39.025, 40.225 and 40.825 to demonstrate that though the sinusoidal is at its hyperpolarizing peak at those time points (note node 25), the dynamic steady state depolarization profile persists. The final plot at 51 ms shows that following block cessation (at 50 ms), the depolarization is diminishing but still present

monotonically, but in a non-linear manner, between 3 to 10 kHz. Between 10 to 40 kHz the block thresholds showed a linear relationship versus frequency (Fig. 3(A)). Block could not be achieved below 2.2 kHz. Instead, the model demonstrated continuous firing of the axon when the current level exceeded the activation threshold. Between 2.2 to 3 kHz, block was obtained only for the larger diameter axons and was accompanied by numerous onset APs. The modeling was performed with the HFAC starting with the first half-cycle being anodic. There were no threshold differences with cathodic first half-cycles.

The block threshold current amplitudes were transformed to threshold charge per phase for each tested frequency (area under the curve of one half-cycle of the sinusoid with units of μC). Figure 3(B) shows the relationship of threshold charge as a function of frequency. The same data is then plotted as a function of the half-cycle pulse width in Figs. 3(C) and (D). Each plot also shows the activation threshold to obtain a single action potential in a 10 μm axon using a single sinusoidal cathodic half-cycle with the half-cycle width determined by the relevant frequency. This demonstrates that block thresholds show trends which are similar to activation of the axon.

Block thresholds and axon diameter

The relationship of block threshold to axon diameter is shown in Fig. 4. Larger axons needed less current to block. The difference in the thresholds for different diameters was influenced by the HFAC frequency. Smaller axons showed a larger threshold difference between different frequencies (higher frequencies always needing larger currents). For the largest diameters, the threshold differences between frequencies were much smaller. At the lowest frequencies (long half-cycle pulse widths), the block threshold was almost independent of diameter (Fig. 4 plot for 3 and 4 kHz). This compares well with the finding that for nerve activation, very long pulse widths show minimum diameter discrimination (Mortimer, 1981).

Block thresholds and electrode distance

The blocking currents were related to the distance between the blocking electrode and the axon (Fig. 5(A)) and varied approximately as the square of the perpendicular distance to the axon. However, when the electrode was closer than 1 mm to the axon, the distance of the electrode to the nearest

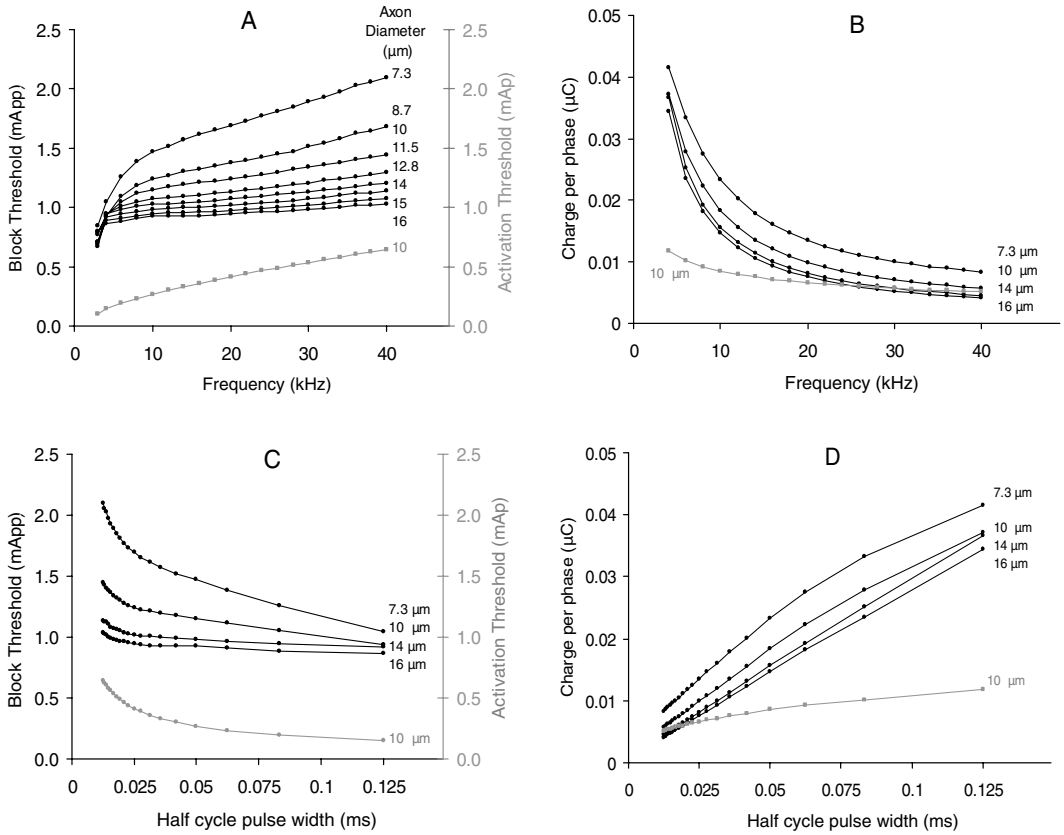

Fig. 3 Block threshold as a function of HFAC sinusoid frequency. (A) shows block threshold in mA (peak to peak) over the frequency range of 3 to 40 kHz for all diameters modeled. No block was obtained below 2.2 kHz. (B), (C) and (D) cover the range of 4 to 40 kHz. (C) shows block threshold for four diameters versus the half-cycle pulse width of the sinusoidal (for 4 to 40 kHz). (B) shows threshold charge-per-phase versus frequency for four diameters and (D) shows threshold charge-per-phase versus the half-cycle pulse width of the sinusoidal. The grey lines in all four plots show the activation threshold (mA peak) or the equivalent charge per phase to elicit a single AP in a 10 μm axon using one cathodic half-cycle of the sinusoidal HFAC at each tested frequency

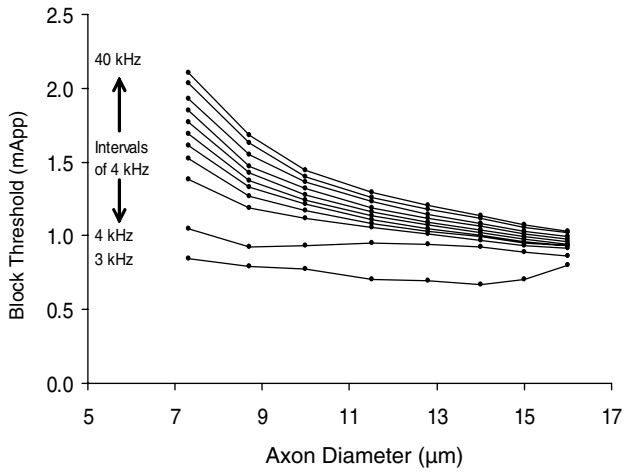

Fig. 4 Block thresholds plotted as a function of axon diameter for frequencies between 3 and 40 kHz. Thresholds are lower for larger diameter axons. At 3 and 4 kHz, there is absence of axon size dependency

node became the predominant factor influencing block threshold. Figure 5(B) shows the effect when the electrode was moved from over the central node to intermediate positions between nodes. For electrode-to-axon distances of less than 1 mm, moving the electrode towards the internodal position increased the block threshold. For example, at an electrode-to-axon distance of 0.1 mm, the block threshold with the electrode at the internodal center was 730% greater compared to being placed over a node, and 140% greater at an electrode-to-axon distance of 0.5 mm. For electrode-to-axon distances of 1 mm or more, the thresholds marginally decreased as the electrode moved towards the internodal position (2% less at an electrode-to-axon distance of 2 mm and 6% less at an electrode-to-axon distance of 1 mm).

HFAC behavior and block onset

The application of HFAC produced a consistent pattern in the axonal response. At very low amplitudes there was a local change in transmembrane voltage, which followed the phases of the HFAC waveform, without producing any APs. As the amplitude was increased there was a threshold at which a single AP could be produced (Fig. 6: line a). This was only possible in the 16 μm axon when the current amplitudes were changed by steps of 0.001 $\times$ block threshold (Fig. 6).

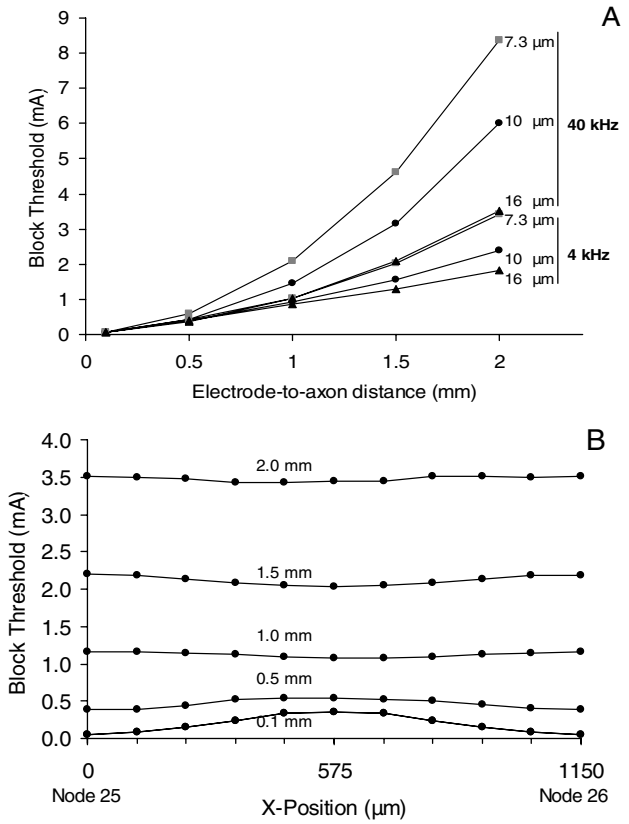

Fig. 5 Block threshold and electrode position. (A) shows block thresholds for three axon diameters at two frequencies and five electrode-to-axon distances. (B) shows block threshold for a 10 μm fiber using a 10 kHz HFAC at five electrode-to-axon distances while the x-position of the electrode is changed from directly over node 25, through 10% displacements (115 μm), to directly over node 26. The internodal distance of the 10μm axon in the model is 1150 μm

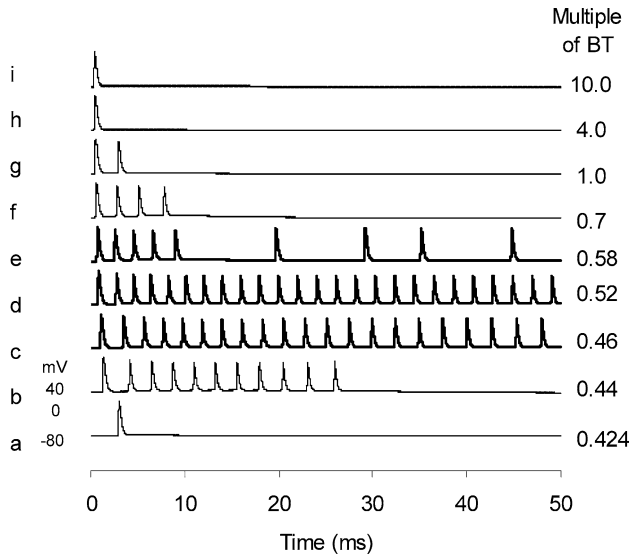

Fig. 6 Onset firing in a 16 μm axon using a 20 kHz HFAC sinusoid at a 1 mm electrode-to-axon distance using current amplitudes which were multiples of the block threshold (0.964 mA). Thick black lines (6 c, d, and e) indicate continuous and infinite firing. At 0.424 $\times$ block threshold (a) there is a single action potential fired. As amplitude is raised, the number and frequency of the firing increases (b, c, and d) and then this trend reverses above 0.52 $\times$ block threshold (e and f) until only 2 action potentials are fired at block threshold (g). At 4 $\times$ and 10 $\times$ block threshold only one action potential is fired (h, i)

More generally, a *finite* burst of APs, at frequencies between 500 to 600 Hz, were produced. With minimal increase in amplitude, the axon continued to respond with *finite* firing that *increased* in frequency as amplitude increased (Fig. 6: line b and Fig. 7). Further increase in amplitude caused a *continuous* firing pattern, at approximately 300 to 450 Hz, with the frequency *increasing* with amplitude (Fig. 6: lines c and d and Fig. 7: black superimposed lines). This was followed by *continuous* firing with a *reduction* in the frequency (Fig. 6 line e and black superimposed lines in Fig. 7). Finally, the number of APs again became *finite* at current levels that were approximately 0.6 to 0.7 times the block threshold (Fig. 6: line f). Further decrease in the number of APs occurred before conduction block was attained at block threshold (Fig. 6: line g). Amplitudes higher than the block threshold maintained the conduction block and decreased the initial number of APs to between one and three (Fig. 6: line h and Fig. 7). It was never possible to obtain a conduction block without firing at least one initial AP. Once block was obtained, all amplitudes above that threshold also produced block with no increase in the initial firing (amplitudes as high as ten times block threshold were tested) (Fig. 6: line h, i). The number of APs at block threshold and higher was also a function of axon diameter, with smaller diameter axons firing more action potentials at block threshold. Typically, the 7.3 μm axon fired five times (Fig. 7(A)) at block threshold and the 16 μm axon fired twice (Fig. 6: line g and Fig. 7(B)). In the smaller axon, the continuous firing at amplitudes below block threshold was higher and over a wider amplitude band. There was a small increase in firing rate at the higher HFAC frequencies which was more marked in the larger diameter fibers.

Mechanism of block

When the HFAC was turned on, it produced large fluctuations in the transmembrane voltage (Fig. 8(A)). However, a region of the axon underneath the electrode was incrementally depolarized with continued delivery of the HFAC (Figs. 2 and 8(A)). This depolarization was initiated by the APs from the onset activity. Finally, a dynamic steady state was reached when the mean transmembrane voltage was maintained at an average depolarized value (Fig. 8(A)). In other words, though the transmembrane potential was oscillating in step with the incident charge-balanced sinusoidal waveform, the oscillations were centered on a depolarized membrane potential and not the resting potential of –80 mV (Fig. 8(A)). Therefore, averaging the membrane potential oscillations over complete

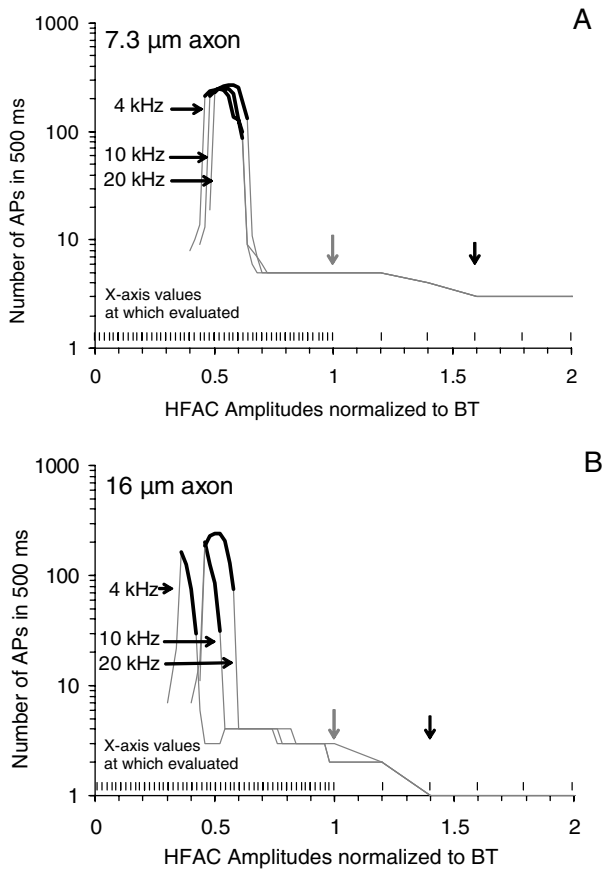

Fig. 7 Onset firing at three HFAC frequencies for two diameters while the amplitude was varied from 0 to 4 × the block threshold (block thresholds varied for each combination of variables). Evaluations were done at a spacing of 0.02 × block threshold between 0 and block threshold and at 0.2 × block threshold between 1 and 4 × block threshold (indicated by the short vertical lines above the X-axis). The data is shown up to 2 × block threshold (there were no differences between 2 and 4 × block threshold). The grey lines indicate the finite number of APs initiated in 500 ms. Thick black lines superimposed on the grey lines indicate continuous firing that continued indefinitely beyond 500 ms. (A) shows the response of a 7.3 μm axon and (B) that of a 16 μm axon. Grey arrows point to the number of onset action potentials at block threshold and the black arrows show the number of APs produced at supra-block threshold

sinusoidal time cycles for every node revealed this dynamic steady state depolarization. The presence of this depolarization was also very evident when the HFAC waveform was turned off, because the offset transmembrane voltages showed a decline towards the normal resting potential, which was reached in approximately 10 ms, for currents just above block threshold (the length of post-block time shown in Fig. 8(A) is 2 ms). This decline occurred even if the waveform was turned off at its *hyperpolarizing peak* (or at any other time) and was also clearly evident in voltage profiles of the paranodes which are minimally influenced by the sinusoidal fluctuations (Kilgore and Bhadra, 2004). At block threshold, the depolarization profile was present over approximately 17 to 25 nodes, while the remaining nodes outside this zone showed a low level of hyperpolarization.

The channel currents showed fluctuations in phase with the incident sinusoidal frequency (Fig. 8(B)). Fast inward sodium currents were larger than outward currents (slow potassium and leakage) (Fig. 8(B)) leading to a net inward current (Fig. 9(E)). This inward current flowed out of the axon through nodes outside the depolarized zone, thus maintaining charge balance in the model. The peak sodium currents in the central node during this dynamic steady state were about 30% of that for a normal action potential (Fig. 8(B) and (E)). The gating variables similarly showed dynamic steady states, with the m parameter fluctuating over a wide range (due to its faster time constant), while the h parameter showed a narrow range of fluctuation around a mean low value (Fig. 8(C) and 9(F)).

Spatial mean nodal voltage profiles along the length of the axon are shown at block threshold in Fig. 9 for a variety of test variables. These spatial profiles reveal that the mean voltage profiles at the respective block thresholds were extremely consistent. The peak average transmembrane voltage at the central node across all of the tested parameters was –48.2 mV (range -52.4 to -46.2 mV), as shown in Fig. 9. Figure 9(A) illustrates profiles for different blocking frequencies and Fig. 9(B) for varying electrode-to-axon distances. Figure 9(C) shows the similarity of the spatial voltage profiles for 3 different axon diameters plotted on an abscissa of node number, also demonstrating that the voltage profiles reached similar peak depolarizations. When graphed on a true millimeter length scale (not shown), the width of the depolarization profile was dependent on the diameter. Smaller axons had a narrower depolarization profile, but the same peak depolarization at the central node.

Figure 9(D) plots voltage profiles for a 10 μm fiber at a 1 mm electrode-to-axon distance using a 10 kHz HFAC at 0.75, 1, 2, and 4 times the block threshold amplitude. The profiles are different from one another, with higher amplitudes producing more depolarization and a broader profile. It is also noteworthy that at 4 times threshold the spatial depolarization covers approximately 31 nodes. It was confirmed that the profiles in a 51 node model showed no differences from a 201 node model.

The ionic currents showed trends that correlated with this spatial voltage profile. Figure 9(E) shows that the average inward sodium current exceeded the average outward potassium current resulting in a net inward current over the depolarized nodes. The capacitance, leakage and slow sodium currents were negligible. The states of the ionic gates also were consistent with these ionic current flows as shown in Fig. 9(F). In the region of the depolarization, the *h* parameter was low, while *m* was high. The s and mp parameters maintained higher than normal dynamic steady states. The *h* and *m* parameter values were thus consistent with a

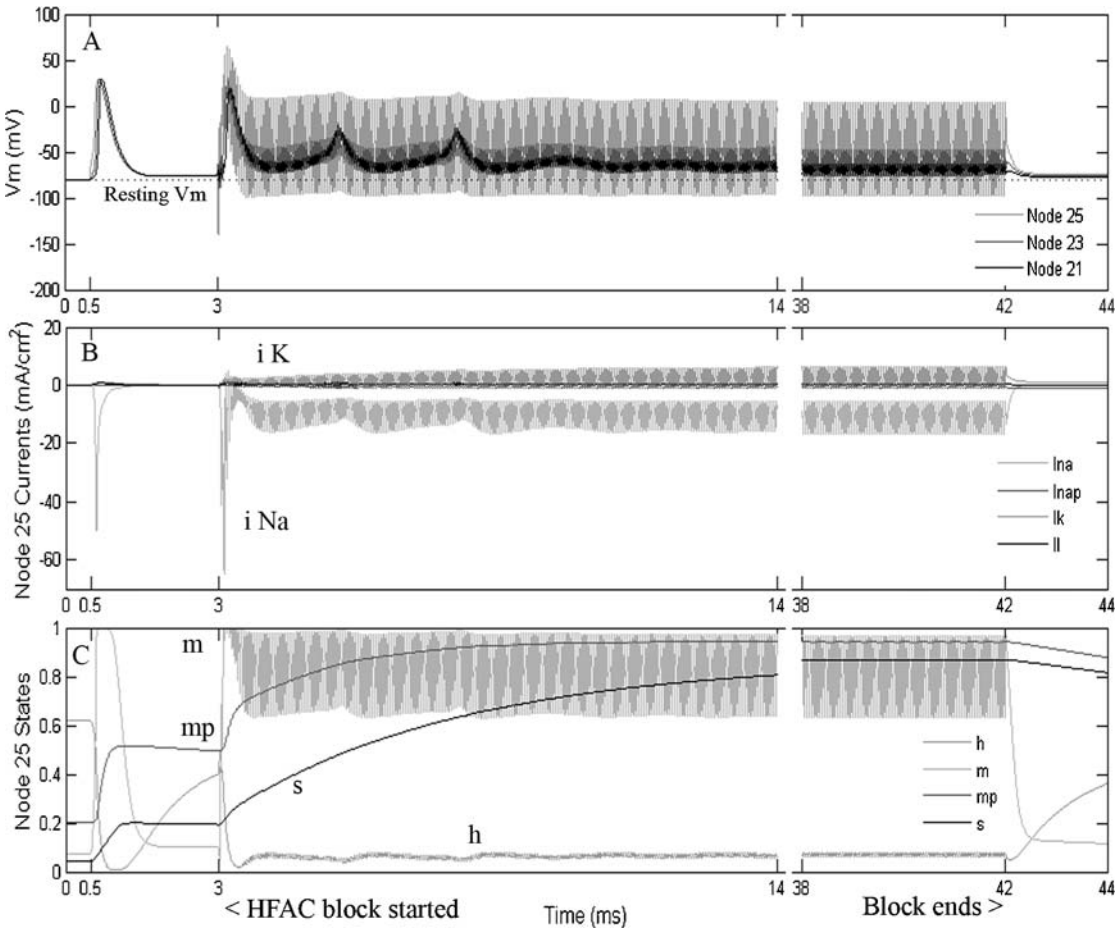

Fig. 8 (A) Transmembrane potentials (nodes 21, 23, 25) (B) currents (node 25) and (C) gating variables (node 25) in a 10 μm axon. For comparison with the HFAC, a single AP is initiated at 0.5 ms in node 25 using an internal electrode (monopolar square pulse, width 0.1 ms, 10 nA). The HFAC block is turned on from 3 ms to 42 ms (1 mm electrode-to-axon distance, 20 kHz, 1.4 mA, $\sim$ 10% above block threshold). Three onset APs are generated. All the variables show dynamic stability between 38–42 ms. The block is turned off at 42 ms and shows the average depolarization declining towards the normal resting potential between 42 and 44 ms. The resting potential is marked by a dashed line in (A)

depolarization mechanism of conduction block where the sodium channels are in a state of inactivation.

Discussion

There are three significant outcomes obtained from the HFAC simulations using the MRG model as detailed in the following paragraphs. First, the model behavior corresponds well to recently published experimental HFAC nerve block results regarding the frequency range at which block occurs, thus further validating the use of this model for HFAC simulation. Second, the characteristics of the onset response have been explored and matched to published experimental data. Third, the mechanism of HFAC block has been examined in terms of the dynamic steady state of the spatial nodal variables at block threshold.

The MRG mammalian model demonstrated conduction block between 3 kHz to the highest frequency of 40 kHz (Fig. 3(A)). This predicted frequency range matches well with previous experimental findings. Bowman and McNeal (1986) demonstrated mammalian nerve block over 4 to 10 kHz (square waveforms with gaps). Motor block was obtained over the range of 10 to 30 kHz (sinusoidal) in the rat sciatic nerve (Bhadra and Kilgore, 2005). HFAC higher than 30 kHz also produced block but were not explored in depth since the maximum blocking voltage was constrained to 10 V_{pp}. At frequencies lower than 10 kHz, continuous tetanic or intermittent contractions of the gastrocnemius muscle were observed. In preliminary experiments, block was obtained as low as 6 kHz but at the expense of prolonged firing. HFAC sinusoidal block of the cat pudendal nerve was achieved using a conforming electrode in the frequency range of 1 to 30 kHz sinusoidal HFAC (Bhadra et al., 2006), with added distal stimulation to confirm conduction block. Williamson and Andrews (2005) obtained block in the rat peroneal nerve between 10 to 20 kHz (sinusoidal). Previously, the MRG model was used with a reduced G_{Na} (to minimize continuous

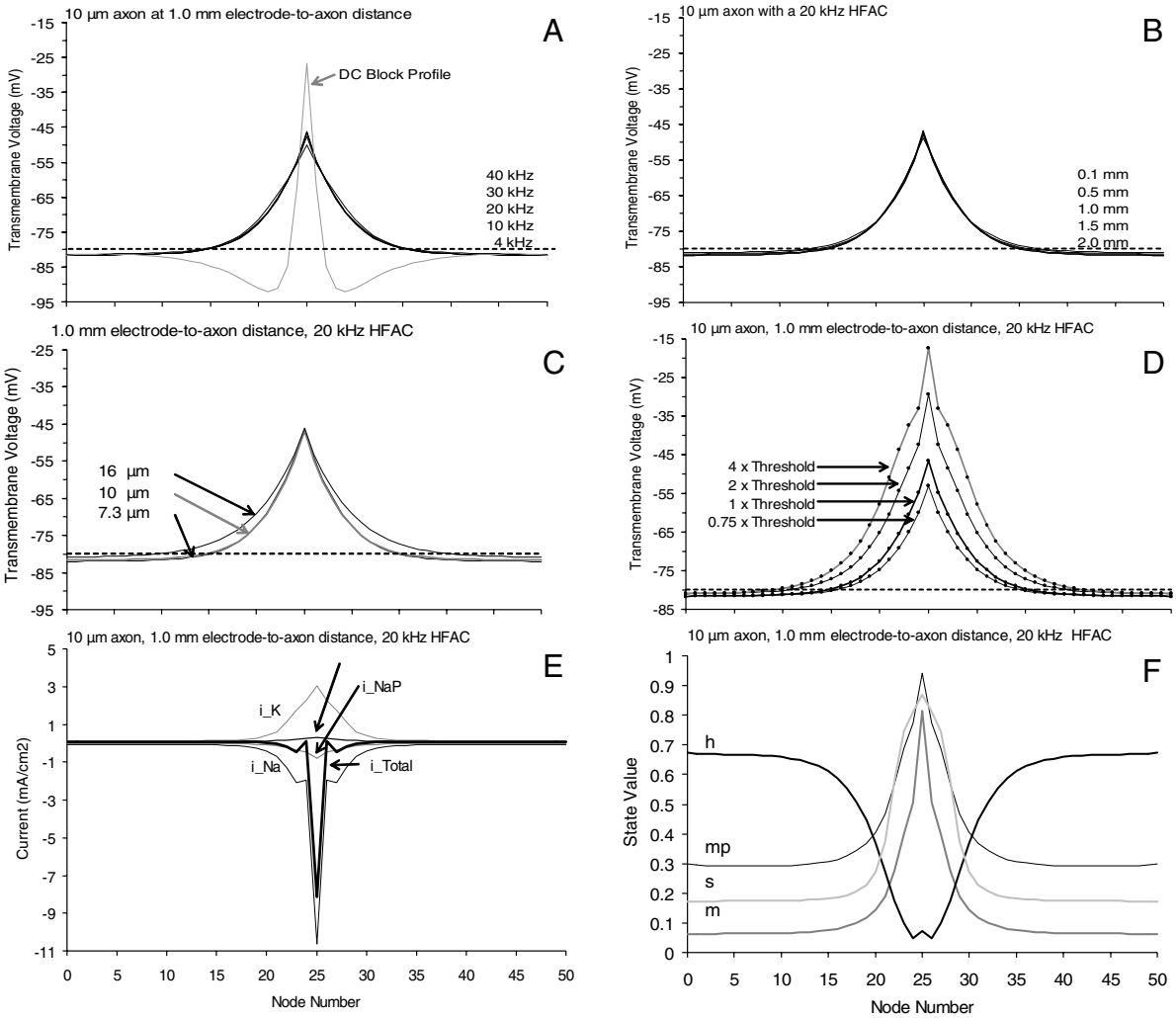

Fig. 9 (A) and (B) show transmembrane voltage profiles at block threshold under different HFAC frequencies and electrode-to-axon distances. All the profiles are similar at block threshold. The transmembrane voltage profile for a DC block (at a cathodic threshold current of 0.307 mA) is added in A to illustrate the differences from HFAC profiles. The DC block shows a narrow depolarization zone and large flanking virtual hyperpolarization zones. (C) shows transmembrane voltage profiles for three diameters at block threshold (20 kHz, 1 mm electrode-to-axon distance). All three reach similar peak depolarization at the central node. (D) shows transmembrane voltage profiles for a 10 μm axon (20 kHz, 1 mm electrode-to-axon distance) using multiples of the block threshold current amplitude (1.244 mA). Changes in amplitude cause changes in both the peak depolarization and the spatial width of the profile. (E) plots all the currents including total current and demonstrates net inward current in and around the central node. (F) plots the gating variables in the model and illustrates that the sodium inactivating parameter "h" is low in and around the central node

firing) and demonstrated block between 3 to 10 kHz (tested up to 10 kHz) (Kilgore and Bhadra, 2004). The only other mammalian simulations performed for HFAC conduction block were in topologically simpler axonal models where block was demonstrated between 5 to 20 kHz in one out of three mammalian models (Williamson and Andrews, 2005). It is likely that block can be obtained above 40 kHz, but this range has not been pursued either experimentally or through simulation.

The identification of the "block threshold" as a measure of HFAC block allows comparisons across variables and studies. Block threshold is easily identified both experimentally and in simulation. Since complete block is always demonstrated at amplitudes above block threshold, as shown by the simulations presented here and by previous experimental results (Kilgore and Bhadra, 2004; Bhadra and Kilgore, 2005; Bhadra et al., 2006), the block threshold identifies an unequivocal boundary in the nerve response to HFAC waveforms. Therefore, the measurement of block threshold in future experiments is strongly encouraged.

The block thresholds from the model showed a linear relationship between 10 to 40 kHz (Fig. 3(A)). Previous experimental results showed a linear relationship of voltage controlled block thresholds to the sinusoidal frequency between 10 to 30 kHz in rat sciatic nerve (Bhadra and Kilgore, 2005) and between 1 to 30 kHz in the cat pudendal nerve (Bhadra

et al., 2006). The block thresholds from the model showed a non-linear relationship to the HFAC frequency between 3 to 10 kHz (Fig. 3(A)). The only repeated and randomized HFAC block threshold data below 10 kHz is from the cat pudendal nerve experiments (Bhadra et al., 2006). These thresholds, where the lowest block frequency achieved was 1 kHz, were fitted linearly (Bhadra et al., 2006). Despite this, Fig. 4 in that paper reveals non-linearity at the lower frequencies, similar to that seen in the model results. We conjecture that there is a single non-linear relationship between block thresholds and frequency over the entire frequency range of block. However, this can be approximated well with a linear fit from 10 kHz upwards. Further experimental data at the lower frequencies are needed to validate this hypothesis. Previous mammalian modeling showed a linear relationship between 5 to 20 kHz in the SRB model but did not show this non-linear relationship below 10 kHz (Williamson and Andrews, 2005).

In rat experiments, the average voltage threshold has been reported to be approximately 3 V_{pp} at 10 kHz and 9 V_{pp} at 30 kHz. Due to the variability in the electrode impedance between animals this corresponded to blocking currents of 1 to 11.8 mA. In the model, the current range across all axon diameters and HFAC frequencies between 3 to 40 kHz, was 0.8 mA to 2.1 (0.93 to 1.89 mA between 10 to 30 kHz for all diameters), for a representative 1 mm electrode-to-axon distance. The lowest current values correspond well between model and experiment. The present model does not incorporate the electrode–tissue interface, or the specific electrode geometry, and these factors are likely to have a significant influence on the electrode impedances. Higher impedances would lead to higher blocking current requirements.

In an attempt to understand the relationship of block threshold to frequency, the activation thresholds to elicit a single AP using one cathodic half cycle of the HFAC were measured and plotted (Fig. 3). Block thresholds versus half-cycle pulse widths (Fig. 3(C)) show similarities to strength-duration activation plots. Likewise, the charge per phase plotted versus the half-cycle pulse width shows similarities to charge-duration plots for nerve activation (Fig. 3(D)). This similarity is hypothesized to be the result of a common mechanism underlying nerve activation and HFAC blocking, namely membrane depolarization. The presentation of future HFAC blocking results in this form will allow comparisons of charge per phase across different blocking modalities, e.g. waveform shape, unbalanced waveforms and discontinuous waveforms. Charge per phase is also likely to be an important criterion in studying the safety of these HFAC waveforms for potential clinical nerve block applications (McCreery et al., 1990).

The model shows that the block thresholds decreased as axonal diameter increased (Fig. 4) over a range of HFAC frequencies (6 to 40 kHz). A similar trend has been shown in mammalian axon models at a single frequency of 10 kHz (Williamson and Andrews, 2005) and also in an unmyelinated Hodgkin-Huxley model in the frequency range of 4.167 to 10 kHz (Tai et al., 2005c). Experimentally, Tanner showed that higher currents were needed to block the smaller fibers in frog sciatic nerve (Tanner, 1962). Woo and Campbell repeated these findings in the frog and also demonstrated similar results in cats (Woo and Campbell, 1964). Compound action potential recordings were used in both these studies and it is possible that some nerve activity cannot be observed due to temporal dispersion of the APs generated by the HFAC. There is no other direct experimental evidence of this relationship of HFAC blocking thresholds to axon diameter.

The block threshold varied as a function of perpendicular distance between the monopolar electrode and the axon and varied inversely as the second power of the distance. This has been previously discussed (Rattay, 1990). As the electrode-to-axon distance decreased below 1 mm, the effect of the electrode position in relationship to the node and internode (x-position, parallel to the axon) became important. Much higher block currents were required at the internodal position. This implies that even at the same electrode-to-axon distance, some larger axons may have a higher block threshold if the electrode is placed between nodes, regardless of the block threshold to diameter relationship. In contrast, when the distance increased to 2 mm, the threshold difference was minimal (2%). We believe this is of significant interest for whole nerve block experiments and possible future clinical applications. Williamson and Andrews (2005) positioned the electrode only over the node or the center of the internode at a single fixed electrode-to-axon distance of 1 mm and noted a 20% decrease in block threshold over the internode.

The model provides insight into the block onset phenomenon and matches experimental data. In the model, as the amplitude of the HFAC was increased, the axonal response showed distinct stages. Low amplitudes produced subthreshold changes without any APs. Experimentally, low amplitude HFAC similarly produces no effects (Bowman and McNeal, 1986). Following this, in the model, a finite burst of APs were produced at a threshold amplitude (Fig. 6). As the current was increased above this level, the APs increased in frequency and became continuous (Fig. 6). In the rat sciatic nerve, as amplitude was increased, the HFAC produced a sudden burst of onset activity. Once block threshold was reached in the model, the axon fired between two to five times, smaller diameter axons tending to be more excitable, while amplitudes higher than block threshold lowered the number of initial APs to one to three. Experimentally, the onset activity in motor block of the rat sciatic nerve showed increased firing at the lower amplitudes which decreased as the amplitude was increased (Bhadra and Kilgore, 2005). The bimodal relationship of the onset firing pattern with

increasing amplitude identified in the MRG model mirrors closely the bimodal firing frequency response of single fibers (alpha motoneurons) to increasing HFAC amplitudes (Bowman and McNeal, 1986). Therefore, the simulation results from the MRG model are consistent with the reported experimental results in mammals.

Karu et al. (1995) showed in human experiments that N-let stimulation (N = a number of rapid stimulation pulses of two or more) resulted in a summation of twitch force which could be as large as six times a normal single muscle twitch (when $N = 6$). The N-let phenomenon is produced by repeated stimulation of the nerve at a high frequency. The onset response is postulated to be a result of the HFAC initially activating the nerve at the maximal rate that the refractory period of the nerve allows, leading to an N-let response in the muscle. The present model results show this type of activity with the number of onset APs being between two and five at block threshold. Onset response force amplitudes in the in-vivo rat experiments were in the range of one to eight times that of single twitch amplitudes (Bhadra and Kilgore, 2005). Bowman and McNeal (1986) identified an initial firing in the nerve at a rate of 500 to 800 Hz during the onset of the block that lasted one to two seconds. This compares well with the $\sim$500 Hz firing frequency that the MRG model shows at frequencies that block (Fig. 7, note that the axis shows firings over 0.5 s). At 1 kHz, a frequency where block was not obtained, the MRG model could maximally fire at 700 Hz. Previously, Williamson and Andrews (2005) reported modeling results from the SRB model where a single AP was first produced, followed by a series of APs as the amplitude of a 10 kHz sinusoid HFAC was increased. The firing frequency increased from 102 to 185 Hz and then abruptly decreased to a single AP. The onset responses from the SRB model are thus considerably less and at lower frequencies than the experimental data of Bowman and McNeal (1986). The SRB model also does not show a bimodal response to increasing amplitude, as found experimentally.

The second phase in the onset phenomenon was a period of tetany or repetitive fasciculations of parts of the muscle (Bhadra and Kilgore, 2005). This activity showed a typical relationship in the HFAC frequency-amplitude space, being decreased with combined higher frequencies and higher amplitudes. The model results show similar trends with the firing frequency and total time of repetitive firing being affected by both the HFAC frequency and the current amplitude (Figs. 6 and 7). Further, the model predicts that smaller axons will show higher onset activity. This remains to be experimentally investigated. The present MRG model does not incorporate the frequency-dependant impedance of the electrode-to-nerve interface, the perineural tissues or an anisotropic extracellular medium and thus cannot completely depict the onset phenomenon. In the future, finite element models of electrodes that have realistic representations of the electrode surface and current distributions, combined with frequency dependant modeling of the extra-axonal impedance, could help fully explain the phenomenon of repetitive firing.

HFAC block produced a dynamic steady state depolarization of the nerve membrane over a broad region (Figs. 2 and 8) which was maintained across multiple nodes (17 to 25 nodes at block threshold). Block did not occur at a single node. Rather, there was progressive attenuation of the action potential as it traversed the dynamically depolarized area, until it was extinguished in the region under the electrode. Spatial transmembrane voltage profiles were essentially identical across a wide range of test variables (HFAC frequency, electrode-to-axon distance, and axon diameter) when the HFAC amplitude was at the block threshold for those variables (Figs. 8 and 9). The nodal currents and the state parameters (Fig. 8) were also consistent with the zone of dynamic depolarization. The important observation is that though all the parameters (transmembrane voltage, nodal currents and gates) fluctuate in phase with the frequency of the blocking HFAC, the net average values are consistent with the maintenance of a zone of depolarization which is sufficient to block APs (Figs. 8 and 9). This occurs despite the fact that there is a zero net charge delivered to the tissue.

Other authors have previously postulated a depolarization mechanism in HFAC conduction block (Tanner, 1962; Williamson and Andrews, 2005). In direct current (DC) nerve block, depolarization of the nerve membrane is known to increase the threshold for activation and produce block (Zimmermann, 1968; Sassen and Zimmermann, 1973; Grill and Mortimer, 1997). DC block experiments and computer simulations demonstrated that DC depolarization block was the prevalent type of DC block (Bhadra and Kilgore, 2004). DC block produces a narrow region of depolarization directly under the electrode flanked by wide and large hyperpolarized regions, known as "virtual electrodes" (Ranck, 1975; Warman et al., 1992) (Fig. 9(A)). Block occurs at the central peak of the depolarized region (true cathodic block). At higher current levels block occurs in the flanking hyperpolarized regions (virtual anodic block) (Bhadra and Kilgore, 2004). Therefore, the topological transmembrane voltage profile in balanced HFAC block is dissimilar to DC block (Fig. 9(A)).

Alternative hypotheses on the mechanism of HFAC nerve conduction block have been published. One hypothesis is that it produces a fast-acting and fast-recovering "neural conduction fatigue" (Forbes and Rice, 1929; Bowman and McNeal, 1986). The physiological basis of this type of fatigue is undetermined. The model reveals that a similar time-dependent frequency reduction of axonal firing may occur at current amplitudes below true conduction block thresholds (Fig. 6 line e). Since the model does not incorporate any fatigue mechanisms, it is possible that the nerve response to a

sub-block threshold HFAC may be one explanation of "neural fatigue". Addition of fatigue processes in the model, such as an increase in extra-axonal potassium concentration during the continued HFAC block, may be helpful in studying the temporal behavior of HFAC block. Another hypothesis is that the HFAC maintains the nerve in a constant refractory state (Krauthamer and Crosheck, 2002). However, this does not match experimental evidence. Nerves can fire APs as fast as 700–800 Hz for brief periods (Woo and Campbell, 1964). Furthermore, in the model as well as experimentally in the rat studies, it was easily possible to fire action potentials during a maintained HFAC block by inducing a small rapid increment of the block current, thereby disproving a constant refractory state. Finally, high activation of potassium channels has been proposed as a mechanism in HFAC conduction block of an unmyelinated axon model based on the Hodgkin-Huxley equations (Tai et al., 2005a), but this is unlikely to be the primary mechanism in mammals, since there are few fast potassium channels in mammalian nodes (Schwarz et al., 1995).

The number of nodes used is an important element in HFAC block modeling since the depolarization profile extends 17 to 21 nodes in the region under the electrode. Traditionally, axon models have used 21 nodes or less. The shorter length results in an exaggerated onset firing (from the two ends of the axon), under-estimation of the block thresholds and in inaccuracies in the electrode-to-axon distance and diameter relationships. In view of this, a 51 node model was adopted for the present study and a 201 node model was used to verify some of the observations.

HFAC waveforms show potential as a method of reversibly blocking conduction in nerve. However, the onset activity produced when the HFAC is initiated is a significant disadvantage for many clinical applications. Accurate computer simulations of the nerve membrane response may enable investigators to develop waveform modifications that eliminate or reduce the onset response.

Acknowledgments This work was supported by the National Institute of Health (NIH) Grant R01-EB-002091 and the State of Ohio Biomedical Research and Technology Transfer Partnership Award BRTT 03-0005. We thank Dr. Cameron C. McIntyre for advice and Angelique Johnson and Alan Barnes for help with the nerve modeling software.

References

Bhadra N, Kilgore KL (2004) Direct current electrical conduction block of peripheral nerve. IEEE Trans. Neural. Syst. Rehabil. Eng. 12: 313–324.

Bhadra N, Kilgore KL (2005) High-frequency electrical conduction block of mammalian peripheral motor nerve. Muscle Nerve 32: 782–790.

Bhadra N, Bhadra N, Kilgore K, Gustafson KJ (2006) High frequency electrical conduction block of the pudendal nerve. J. Neural. Eng. 3: 180–187.

Bowman BR, McNeal DR (1986) Response of single alpha motoneurons to high-frequency pulse trains. Firing behavior and conduction block phenomenon. Appl. Neurophysiol. 49: 121–138.

Forbes A, Rice LH (1929) Quantitative studies of the nerve impulse IV. Fatigue of the peripheral nerve. Am. J. Physiol. 90: 119–145.

Grill WM, Mortimer JT (1997) Inversion of the current-distance relationship by transient depolarization. IEEE Trans. Biomed. Eng. 44: 1–9.

Hines ML, Carnevale NT (1997) The NEURON simulation environment. Neural. Comput. 9: 1179–1209.

Hodgkin AL, Huxley AF (1952) A quantitative description of membrane current and its application to conduction and excitation in nerve. J. Physiol. 117: 500–544.

Kilgore KL, Bhadra N (2004) Nerve conduction block utilising high-frequency alternating current. Med. Biol. Eng. Comput. 42: 394–406.

Krauthamer V, Crosheck T (2002) Effects of high-rate electrical stimulation upon firing in modelled and real neurons. Med. Biol. Eng. Comput. 40: 360–366.

McCreery DB, Agnew WF, Yuen TG, Bullara L (1990) Charge density and charge per phase as cofactors in neural injury induced by electrical stimulation. IEEE Trans. Biomed. Eng. 37: 996–1001.

McIntyre CC, Richardson AG, Grill WM (2002) Modeling the excitability of mammalian nerve fibers: influence of afterpotentials on the recovery cycle. J. Neurophysiol. 87: 995–1006.

Mortimer JT (1981) Motor prostheses. American Physiology Society, Bethesda, MD.

Ranck JB Jr (1975) Which elements are excited in electrical stimulation of mammalian central nervous system: a review. Brain Res. 98: 417–440.

Rattay F (1990) Electrical Nerve Stimulation. Springer-Verlag, Vienna, Austria.

Rattay F (1990) Electrical Nerve Stimulation; Theory, experiments and applications. Springer-Verlag, New York.

Richardson AG, McIntyre CC, Grill WM (2000) Modelling the effects of electric fields on nerve fibres: influence of the myelin sheath. Med. Biol. Eng. Comput. 38: 438–446.

Sassen M, Zimmermann M (1973) Differential blocking of myelinated nerve fibres by transient depolarization. Pflugers. Arch. 341: 179–195.

Sawan M, Hassouna MM, Li JS, Duval F, Elhilali MM (1996) Stimulator design and subsequent stimulation parameter optimization for controlling micturition and reducing urethral resistance. IEEE Trans. Rehabil. Eng. 4: 39–46.

Schwarz JR, Reid G, Bostock H (1995) Action potentials and membrane currents in the human node of Ranvier. Pflugers. Arch. 430(2): 283–292.

Solomonow M, Eldred E, Lyman J, Foster J (1983) Control of muscle contractile force through indirect high-frequency stimulation. Am. J. Phys. Med. 62: 71–82.

Tai C, Roppolo JR, de Groat WC (2005a) Response of external urethral sphincter to high frequency biphasic electrical stimulation of pudendal nerve. J. Urol. 174(2): 782–786.

Tai C, de Groat WC, Roppolo JR (2005b) Simulation analysis of conduction block in unmyelinated axons induced by high-frequency biphasic electrical currents. IEEE Trans. Biomed. Eng. 52: 1323–1332.

Tai C, de Groat WC, Roppolo JR (2005c) Simulation of nerve block by high-frequency sinusoidal electrical current based on the Hodgkin-Huxley model. IEEE Trans. Neural. Syst. Rehabil. Eng. 13: 415–422.

Tanner JA (1962) Reversible blocking of nerve conduction by alternating current excitation. Nature 195: 712–713.

Warman EN, Grill WM, Durand D (1992) Modeling the effects of electric fields on nerve fibers: determination of excitation thresholds. IEEE Trans. Biomed. Eng. 39: 1244–1254.

Williamson RP, Andrews BJ (2005) Localized electrical nerve blocking. IEEE Trans. Biomed. Eng. 52: 362–370.

Woo MY, Campbell B (1964) Asynchronous firing and block of peripheral nerve conduction by 20 Kc alternating current. Bull. Los Angel Neuro. Soc. 29: 87–94.

Zimmermann M (1968) Selective activation of C-fibers. Pflugers. Arch. Gesamte. Physiol. Menschen. Tier. 301: 329–333.